Phase Behavior and Dynamics of the ABA Triblock Copolymer Poly(ethylene glycol) Distearate Doped with Alkali Metal Salts

M. V. Giotto,[†,$] C. L. Sangiorge,[‡] D. J. Harris,[§,&] A. L. deOliveira,[⊥] K. Schmidt-Rohr,[#] and T. J. Bonagamba*[,†]

Instituto de Física de São Carlos, USP, Caixa Postal 369, CEP: 13560-970, São Carlos, SP, Brazil; Departamento de Química, ICEx, UFMG, Caixa Postal 702, CEP: 30161-970, Belo Horizonte, MG, Brazil; Polymer Science and Engineering Department, University of Massachusetts, Amherst, Massachusetts 01003; Departamento de Física, ICEx, UFMG, Caixa Postal 702, CEP: 30161-970, Belo Horizonte, MG, Brazil; and Department of Chemistry and Ames Laboratory, Iowa State University, Ames, Iowa 50011

Received March 26, 2001

ABSTRACT: The ABA triblock copolymer poly(ethylene glycol) distearate (PEGD), average M_n ca. 930, complexed with lithium and sodium perchlorates has been studied by ^{1}H, ^{7}Li, ^{13}C, and ^{23}Na solid-state nuclear magnetic resonance (NMR), SAXS, DSC, and polarized-light optical microscopy. Unlike other solid polymer electrolytes, highly Li^+-doped PEGD samples exhibit sharp ^{7}Li NMR quadrupolar powder patterns even at temperatures well above the melting point, indicating that this triblock copolymer is microphase separated and the dynamics in the PEG phase are anisotropic. Measurements of the ^{7}Li central transition line width in highly doped samples show three distinct line narrowings, due to the poly(ethylene glycol) glass transition (∼−20 °C), the stearate melting point of the polymer (∼35 °C), and an order−disorder transition (∼72 °C). ^{23}Na NMR measurements yield similar results. SAXS, DSC, and optical microscopy with polarized light confirm the presence of a microphase-separated state up to ∼72 °C. ^{13}C and ^{1}H NMR show that the segmental mobility in the ordered state is reduced compared to the isotropic melt. The results confirm the previously proposed order−disorder model to explain the dependence of the ionic conductivity on the lithium concentration for Li^+-doped PEGD samples.

Introduction

The alkali metal ion doped ABA triblock copolymer poly(ethylene glycol) distearate (PEGD), $CH_3(CH_2)_{16}CO(OCH_2CH_2)_nO_2C(CH_2)_{16}CH_3$, average M_n ca. 930, has been studied during the past few years by several experimental techniques including ionic conductivity, thermal analysis (DSC), Raman spectroscopy, viscometry, and NMR.[1−5] The PEGD structure consists of two nonpolar aliphatic stearate sections that have fairly rigid crystalline structures and a more mobile phase composed of the polar ethylene glycol segments. Undoped material has the consistency of a soft wax at room temperature, undergoing a glass transition at −68 °C and a melting transition to a viscous liquid around 35 °C. This material is promising for practical applications due to enhanced mechanical properties with little sacrifice of ionic conductivity.

The polar ethylene glycol segments can dissolve alkali metal salts like lithium and sodium perchlorates, $LiClO_4$ and $NaClO_4$. The concentration of the alkali metal ions (Me^+), Li^+ or Na^+, in the sample is calculated as the oxygen-to-Me^+ ratio, y, where the oxygens considered are only those of the ethylene glycol segments. The thermal behavior, ionic conductivity, and liquid viscosity are known to depend strongly on the O/Me^+ ratio.[1,3−5] As for other polymeric ionic conductors,[6] the doped PEGD samples exhibit an increase in the glass transition temperature with increasing ionic concentration, while the stearate melting temperature remains approximately constant.[4] The alkali metal ion (Li^+ or Na^+) concentration dependence of the ionic conductivity at 50 °C (above the polymer melting point) goes through a very sharp peak, where the ionic conductivity reaches values of approximately 8.0×10^{-4} S/cm (for Li^+−PEGD) and 1.3×10^{-4} S/cm (for Na^+−PEGD) for $y = 9$.[1,4,5] For these ABA triblock ionic conducting copolymers, a special model was proposed on the basis of the order−disorder transition to explain the ionic conductivity behavior as a function of the alkali metal ion concentration above the melting point.[4,5]

To further explore this model, we have performed ^{1}H, ^{7}Li, ^{13}C, and ^{23}Na solid-state NMR measurements on PEGD doped with Li^+ and Na^+ with several O/Me^+ ratios. The temperature dependencies further elucidate the relationships between the cation−polymer interaction and the bulk properties. Additionally, SAXS, DSC, and polarized light optical microscopy experiments have been conducted to complement the conclusions obtained from the NMR experiments.

Experimental Section

Sample Preparation. Commercial poly(ethylene glycol) distearate (PEGD), average M_n ca. 930, lithium and sodium perchlorates, all from Aldrich, were used as received for the preparation of the samples. To obtain the desired ratios of oxygen to Me^+, the complexes were prepared by direct dissolution at 80 °C under vigorous stirring of appropriate amounts of $LiClO_4$ or $NaClO_4$ in PEGD.[1] The Li^+- and Na^+-doped PEGD samples were prepared with $y = 5$, 6, 7, 8, 9, 10, 11, 12, and 50. Immediately after preparation, the samples

[†] USP.
[‡] Departamento de Química, ICEx.
[§] University of Massachusetts.
[⊥] Departamento de Física, ICEx.
[#] Iowa State University.
[$] Present address: Carlson School of Chemistry, Clark University, Worcester, MA 01610.
[&] Present address: Factory Mutual Research, 1151 Boston-Providence Highway, Norwood, MA.
* To whom correspondence should be addressed. E-mail: tito@if.sc.usp.br.

10.1021/ma010515q CCC: $22.00
Published on Web 03/16/2002

were encapsulated in sealed NMR tubes, SAXS sample holders, or DSC Al pans. For the sake of comparison, poly(ethylene glycol) (average M_n ca. 400) (PEG) from Aldrich was also doped with an oxygen-to-Li^+ ratio equal to 5.

Polarized Light Microscopy (PLM). PLM pictures were obtained using a Leica DMRXP polarized light microscope and a hot stage Linkam THMS 600.

Differential Scanning Calorimetry (DSC). DSC measurements were performed with 10 mg samples loaded in Al pans on a DuPont Instruments DSC 2910 equipment. Samples were heated at 10 °C/min from 10 to 90 °C.

Small-Angle X-ray Scattering (SAXS). SAXS measurements were carried out utilizing a Rigaku 18 kW rotating anode (Cu target), using the Ni-filtered Cu Kα line (1.54 Å), and a Siemens area detector.

Solid-State NMR. Static ^1H, ^7Li, ^{13}C, and ^{23}Na NMR spectra were recorded between −100 and 90 °C at 2 T using a TECMAG LIBRA system and a variable temperature double-resonance Doty probe. For all nuclei the static spectra were obtained from the Fourier transform of the free induction decays (FIDs) following a single 8 μs $\pi/2$ excitation. The ^7Li and ^{23}Na spectra were acquired without proton decoupling, while the ^{13}C spectra were always obtained with proton decoupling. The line widths are reported as full widths at half-height and will be referred simply as the line width, $\Delta\nu$. Magic-angle spinning was employed for the temperature-dependent ^{13}C experiments dedicated to measure the isotropic chemical shift and spin−lattice relaxation below the PEGD melting point. The ^7Li and ^{23}Na spin−lattice relaxation times T_1 were measured by the inversion−recovery method.[7] Proton decoupling was used during ^7Li and ^{23}Na FID acquisitions to improve the sensitivity of the experiment, thus allowing T_1 measurements over an extended temperature range. Special care was taken to avoid the sample heating due to radio-frequency irradiation by using pulse sequences with long repetition times (>3 s) and minimizing the number of scans.

Results and Discussion

Polarized Light Microscopy (PLM). The PLM photographs, shown in Figure 1, for the pure and doped (y = 5 and 16) PEGD indicate the presence of crystallinity below the melting point (∼35 °C) for all samples. Figure 1 also shows that, only for the sample with higher lithium concentration (y = 5), order persists above the melting point of 35 °C, and transmitted light remains visible until above 80 °C.

Differential Scanning Calorimetry (DSC). Figure 2 shows the DSC thermograms recorded in the range 10−90 °C for pure and Li^+-doped PEGD samples with y = 5 and 16. It shows the characteristic DSC behavior of pure PEGD, where the large endotherm peak at 42 °C corresponds to the melting of the crystalline regions. For relatively low Li^+ concentration (y = 16), similar behavior is also observed. However, for the highest Li^+ concentration (y = 5) an additional small transition appears at 72 °C, which indicates order induced by the high lithium concentration (y < 9).

A more detailed DSC study of the glass transition of pure and Li^+- and Na^+-doped PEGD samples was done elsewhere,[4] indicating that the presence of alkali metal ions displaces the glass transition to higher temperatures. These data will be compared with the glass transition temperatures obtained from ^7Li line width measurements.

Small-Angle X-ray Scattering (SAXS). The SAXS data, shown in Figure 3, indicate diffraction peaks around 2θ = 2.1° at the temperature of 50 °C, demonstrating the presence of long-range order with a long period of 40−43 Å for the Li^+-doped samples (y = 5, 7, 9, 12, and 16) above the stearate melting point. This peak is absent for the pure sample. In the same figure,

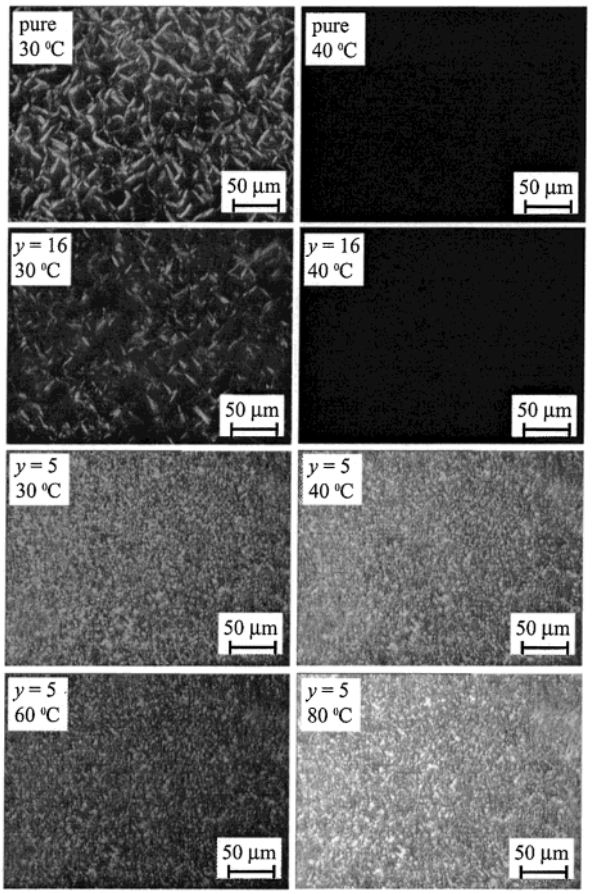

Figure 1. Polarized optical microscopy pictures below and above the melting point (35 °C) for pure PEGD and two Li^+-doped PEGD materials (y = 5 and 16).

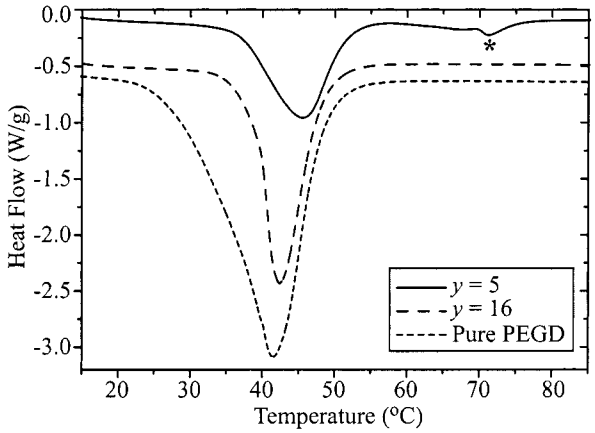

Figure 2. Differential scanning calorimetry traces for pure and for Li^+-doped (y = 5 and 16) PEGD materials. Samples were heated at a rate of 10 °C/min.

it can also be observed that the peaks for samples with $y \geq 9$ are both weak and broad, indicating the lack of strong ordering (disorder). The disorder for the samples with low lithium concentration ($y \geq 9$) is consistent with the absence of birefringence observed by PLM. For y < 9, the peaks are very intense and narrow, indicating a high degree of order. This order−disorder transition around y = 9 occurs at the same lithium concentration as the previously observed peak in ionic conductivity at 50 °C.[1−5]

Figure 4 shows the temperature dependence of the SAXS diffraction intensities around 2.1° for the pure and doped samples (y = 5, 7, 9, 12, and 16). As can be

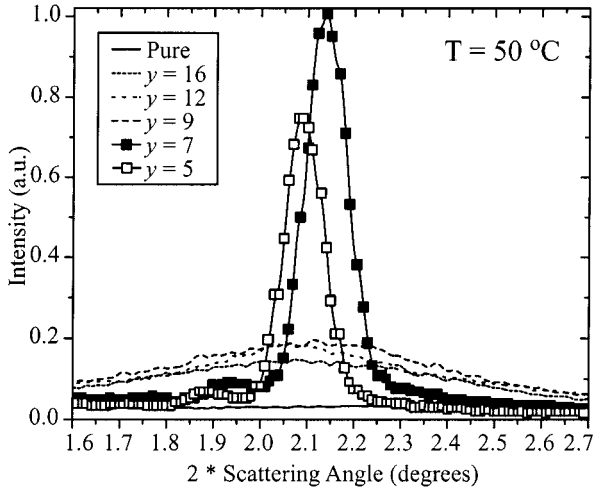

Figure 3. SAXS curves of pure and Li^+-doped (y = 5, 7, 9, 12, and 16) PEGD at 50 °C. The small-angle X-ray patterns indicate an order−disorder transition around y = 9.

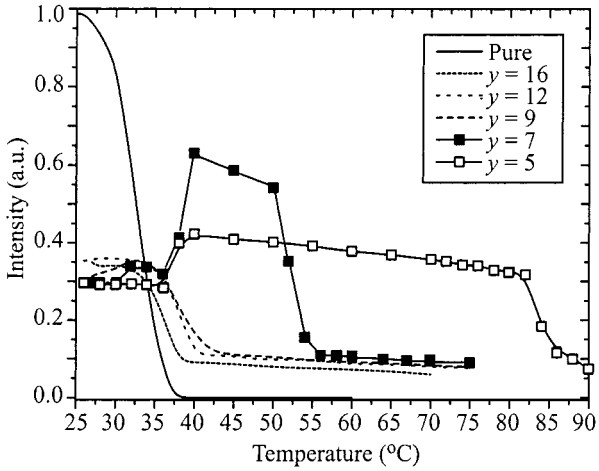

Figure 4. SAXS peak intensities of pure and Li^+-doped PEGD (y = 5, 7, 9, 12, and 16) vs temperature.

seen for samples with $y \geq 9$, the SAXS patterns show weak and broad lines (disorder) well above the melting temperature (35 °C). In the case of samples with $y < 9$, the SAXS patterns are very intense and narrow, indicating order up to temperatures well above the stearate melting temperature. The intense and narrow SAXS peaks persist up to a doping-dependent temperature. The apparent order−disorder transition occurs at 52 and 84 °C for samples with y = 7 and 5, respectively.

^{7}Li NMR. ^{7}Li is a spin-$^3/_2$ nucleus and therefore has a quadrupole moment which in an electric field gradient produces a quadrupole satellite splitting, ν_Q (see Figure 5). In an isotropic melt, motional averaging removes this splitting. Below the glass transition temperature, the ^{7}Li spectra for all Li^+-doped PEGD samples exhibit only a broad line. Above the glass transition and below the melting temperatures, additionally to the central transition, it can be also observed for all Li^+-doped PEGD samples a typical quadrupole powder pattern associated with the satellite splitting (see Figure 5). However, above the melting temperature, only the samples with $y \leq 9$ show the satellite splittings. Therefore, the observation of a quadrupole splitting above the melting is proof of anisotropic dynamics for some of these samples ($y \leq 9$). In contrast, the doped PEG (y = 5) exhibits only the central transition at all temperatures

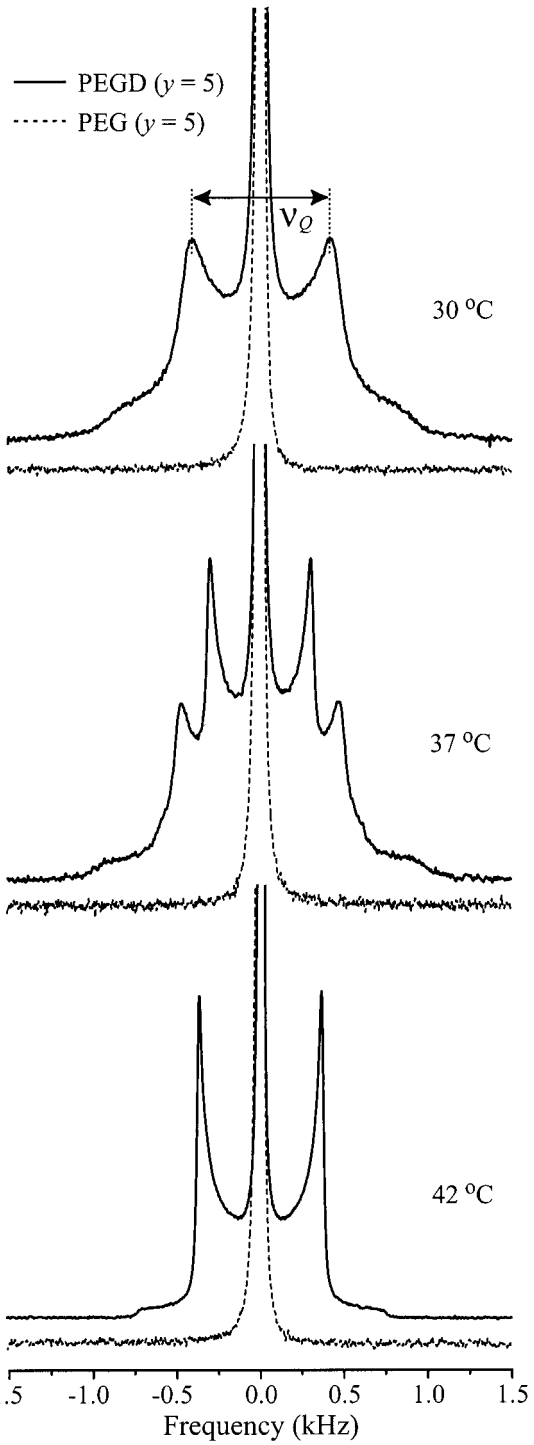

Figure 5. ^{7}Li spectra showing the typical quadrupole powder pattern obtained at three different temperatures, below (30 °C), around (37 °C), and above the melting point (42 °C) for PEGD and PEG, both with y = 5.

used in this study. Typical ^{7}Li spectra of Li^+-doped PEGD and PEG are shown in Figure 5.

The ^{7}Li central transition line width, $\Delta\nu$, the spin−lattice relaxation rate, T_1^{-1}, and the quadrupole splitting, ν_Q, were studied as a function of temperature from −100 to 90 °C for samples with various y values. Typical results of these temperature dependences are shown in Figure 6 for PEGD and PEG, both with y = 5. Measurement of the ^{7}Li central transition line width for PEGD with y = 5 shows three steps at −20, 35, and 72 °C. The first two transitions, at −20 and 35 °C, are

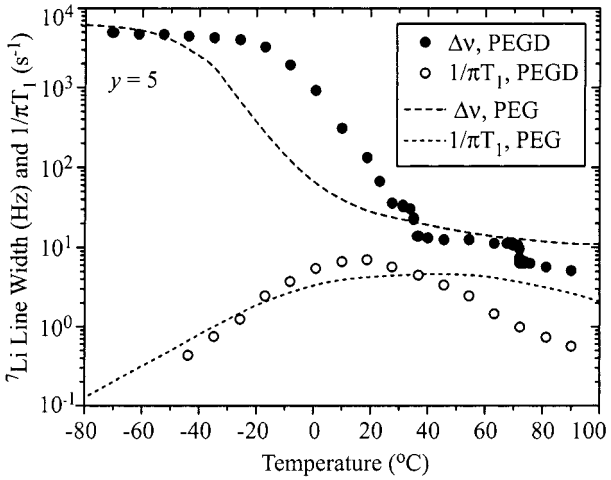

Figure 6. Temperature dependence of the ^{7}Li spin−lattice relaxation rate and line width for PEGD and PEG, both with $y = 5$.

associated with the peaks observed in the DSC traces that are attributed to the PEGD glass transition, T_g, and the melting point, T_m, respectively. The transition occurring around 72 °C corresponds to the transitions also observed by DSC and SAXS, which were assigned to the order−disorder transition. The results of the ^{7}Li spin−lattice relaxation rate measurements for the central transition are also shown in Figure 6 for the same samples, where they were plotted as $(\pi T_1)^{-1}$ in order to estimate the ^{7}Li line broadening due to the maximization of the relaxation rate ($(\pi T_1)^{-1} \approx \Delta\nu$).[7] The maximum ^{7}Li spin−lattice relaxation rate for PEGD with $y = 5$ occurs around 17 °C and is a factor of 10 less than the line width. Thus, the contribution from spin−lattice relaxation rate to the line width is negligible. This is in contrast with ^{23}Na NMR of the polymer complexes prepared with sodium instead of lithium, shown below. The ^{7}Li line width measurements vs temperature for PEG homopolymer with $y = 5$ show no steps above 10 °C.

Similar ^{7}Li line width and spin−lattice relaxation temperature dependences were also observed for PEGD samples with $y = 6$ to 12 and 50 (Figure 7). Glass and melting transitions can be readily observed in almost all samples. The third transition, assigned to the order−disorder transition, was also apparent for the samples with $y = 6$ and 8, around 64 °C. This transition was also faintly distinguishable for the sample $y = 7$, though mixed with the end of the melting transition around 55 °C. As shown later, the third transition for the sample $y = 7$ will be confirmed through the quadrupolar splitting data. Consistent with the PLM and DSC data, samples with $y \geq 9$ did not show the third transition associated with an order−disorder transition. It can be also observed from Figure 7 that the presence of the alkali ion affects the polymer chain motion,[4] where the glass-transition line-narrowing phenomenon is displaced continuously to higher temperatures with the decrease of the oxygen-to-Li$^+$ ratio.

The strongest ^{7}Li line width change shown in Figure 7 can also provide the glass-transition temperatures. This parameter was obtained as the inflection point (on a linear scale) of the ^{7}Li line width curve and termed T_g^{NMR} in order to differentiate it from the DSC T_g. For samples with y ranging from 9 to 50 the maximization of the spin−lattice relaxation rate slightly broadens the

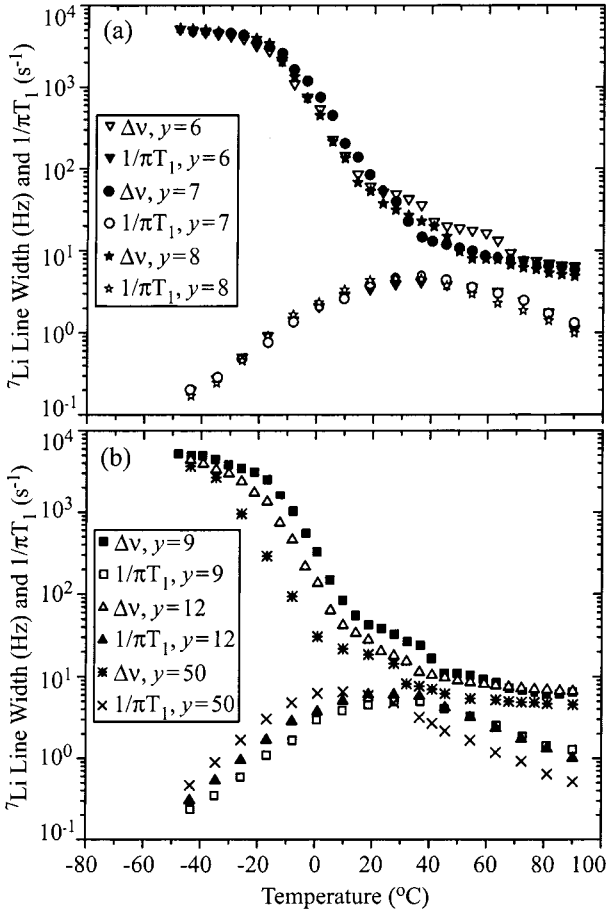

Figure 7. Temperature dependence of the ^{7}Li spin−lattice relaxation rate and line width for PEGD samples with (a) $y = 6$, 7, and 8 and (b) 9, 12, and 50.

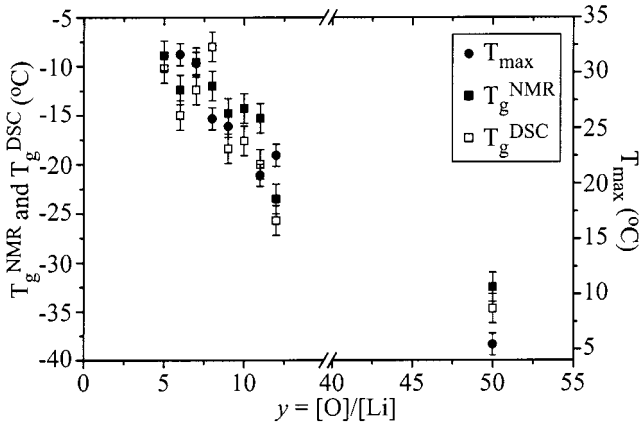

Figure 8. y dependence of the glass transition temperatures determined from DSC and ^{7}Li NMR experiments. For the sake of comparison, the temperature of the maximum spin−lattice relaxation rate, T_{max}, is also shown.

^{7}Li line width (Figure 7b). Another parameter obtained from Figure 7 is the temperature where the spin−lattice relaxation rate reaches a maximum, T_{max}. Both T_g^{NMR} and T_{max} are plotted in Figure 8 together with the glass transition temperatures obtained from DSC experiments in order to show the correlation between both techniques. As observable in Figure 8, a greater lithium concentration results in both higher glass transition temperatures and T_{max}, indicating that the complexation between lithium and the PEG block decreases the polymer mobility.[6]

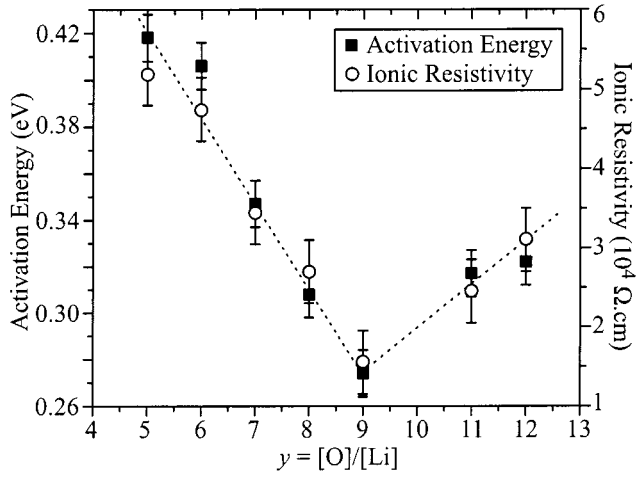

Figure 9. *y* dependence of the activation energy obtained from the ^{7}Li spin−lattice relaxation rate measurements vs temperature and the ionic resistivity obtained elsewhere.[1,4]

The activation energy, E_a, is another important dynamic parameter that can be indirectly obtained from the NMR data. This parameter can be estimated using the Bloembergen, Purcell, and Pound (BPP) model and the Arrhenius law.[8−11] Using the well-known procedures for the determination of the activation energies,[12−14] E_a can be evaluated for the spin−lattice relaxation process. To compare E_a with the conductivity measurements done at 50 °C, the values of E_a were calculated for different *y* values from T_1^{-1} in the temperature interval above T_{max}. The *y* dependence of these activation energies shows a strong correlation with the ionic resistivity reported elsewhere,[1,4] as shown in Figure 9. It is well-known that the cation (Li^+) mobility is directly modulated by the polymer chain dynamics,[12,15−23] and therefore ionic conductivity is mainly confined to the amorphous phase. Ratner and co-workers[24] have proposed a model for long-range transport of cations in polymer electrolytes based on the cation percolation between different sites along the polymer backbone. In this dynamic bond percolation theory, the available sites are constantly appearing and disappearing because of the rapid transformations of the polymer. Therefore, making and breaking of cation−ether oxygen bonds at a high rate is necessary for high cation mobility. For this reason, it is very important to suppress the crystalline phase or local order of the solid polymer electrolytes and use them well above the glass transition, where the polymer mobility is very high.[22,23,25] From this point of view, one should expect a strong correlation between the activation energy necessary to thermally activate the ion motion (or polymer dynamics) and the ionic resistivity, both measured in the same temperature range. The higher the activation energy, the higher is the resistivity of the ionic conductor, like it was demonstrated in Figure 9.

The temperature dependence of satellite quadrupole splitting ν_Q is shown for all samples in Figure 10. In particular, the quadrupolar splitting information for the sample with $y = 5$ was obtained in greater detail. In general, the satellite quadrupolar lines become visible around 10 °C, when the central transition line width falls below approximately 100 Hz due to the onset of motional narrowing above the glass transition (Figures 6 and 7). Taking as an example the PEGD sample with $y = 5$, this low-temperature splitting starts at a value of 770 Hz and slowly increases with temperature up to

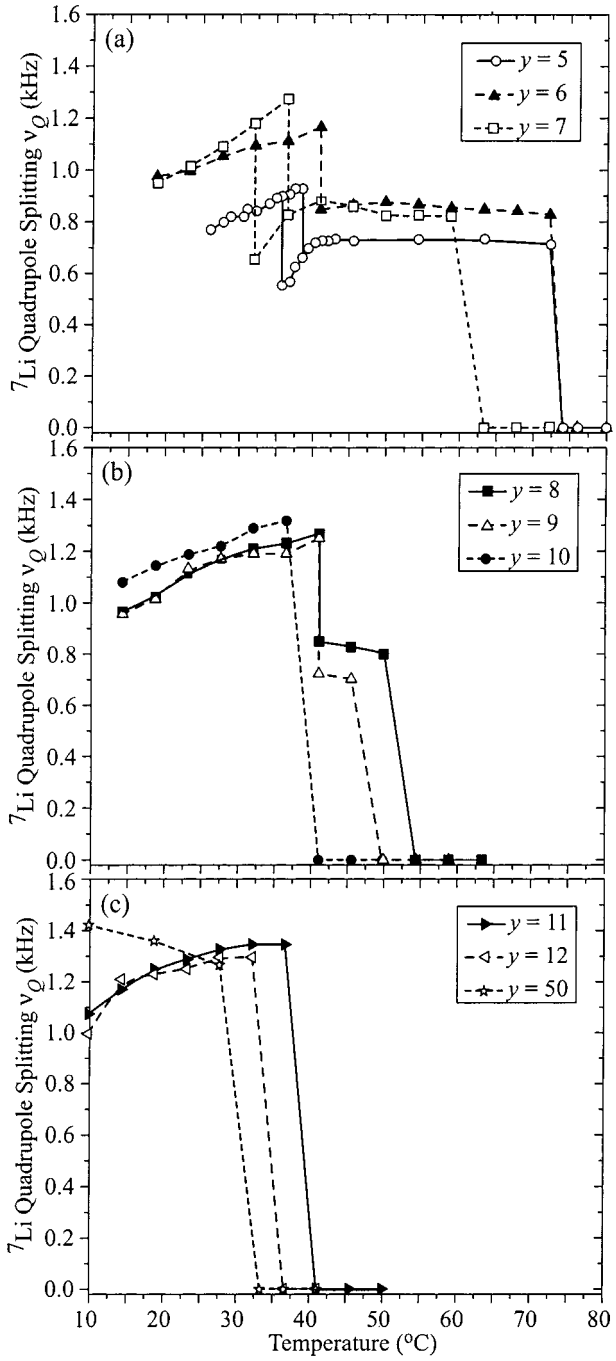

Figure 10. ^{7}Li quadrupolar splitting as a function of temperature for PEGD samples with $y =$ (a) 5, 6, 7, (b) 8, 9, 10, and (c) 11, 12, 50. Note the coexistence of two splittings near 35 °C for $y = 5$ and 7.

a value of 935 Hz near the 35 °C melting point, around which the spectra begin to show simultaneously an additional pattern with a smaller splitting of 555 Hz (Figure 10). Inside the melting region, the splitting of this additional satellite quickly increases to about 730 Hz around 43 °C and then remains slightly constant above the melting point up to 72 °C, when it collapses. The biphasic behavior observed in a narrow temperature range around the melting temperature is not unexpected in this polydisperse material. Temperature gradients can be ruled out as a possible explanation because the NMR tube is small, and the observed splitting did not change even after extended time. In fact, all the spectra were acquired after hundreds of

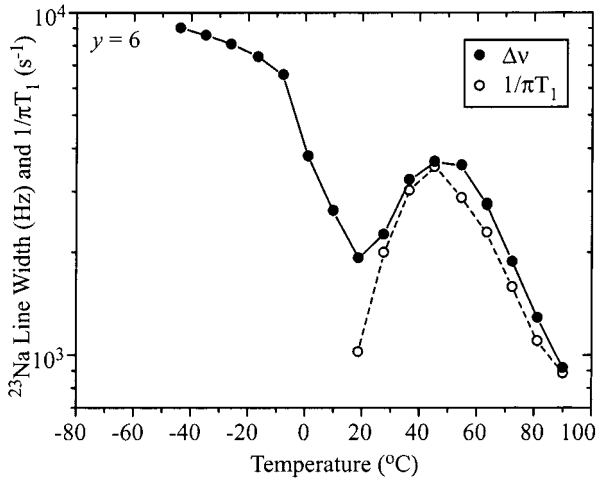

Figure 11. Temperature dependence of the ^{23}Na spin−lattice relaxation rate and line width for PEGD with $y = 6$.

scans with recycle delays of seconds. The possible explanation for this biphasic behavior is the coexistence of the crystalline (stearate) and long-range order (induced by Li^+) phases around the melting temperature. We do not have an explanation for the observed increase of the satellite quadrupole splitting with temperature, in the interval below and around T_m. However, similar behavior was observed and discussed in the ref 26 for crown ether−salt complexes. In that case, in the temperature range 27−87 °C, the quadrupole coupling constant increased steadily with rising temperature from 60 to 68 kHz. Halstead,[27] in a study of atomic motion in $LiNbO_3$, generalized that an increase in the quadrupole coupling constant of a light atom is to be expected if the environment of the nucleus is such that it can vibrate anisotropically. However, there also exist other mechanisms to cause a positive temperature dependence: (a) a change in the electric field caused by changes in the atomic coordinates, (b) a change in the electric field caused by a modification in the electron density distribution, or (c) a change in the time average of the electric field gradient as sampled by the moving nucleus.

Above the melting point, these reduced satellite splittings disappear for all samples with $y > 9$ and remain visible for all samples with $y \leq 9$. The satellite splittings observed above the melting point for samples with $y \leq 9$ remain essentially constant with temperature, until they collapse around 46, 50, 59, 72, and 72 °C for the samples with $y = 9$, 8, 7, 6, and 5, respectively. This shows that the temperature of the collapse of the satellite lines increases with the lithium concentration. The satellite splittings observed below the melting point for the samples with $y < 9$ also show a y-dependent temperature collapse around the following values 28, 32, and 36 °C for the samples with $y = 50$, 12, and 11, respectively.

The information obtained from the temperature dependence of the quadrupole satellites is completely consistent with the DSC and SAXS observations, confirming the order−disorder transition.

^{23}Na NMR. The ^{23}Na spectra consist, for all temperatures, of single broad featureless Gaussian-shaped lines. The typical temperature dependence of the line width and spin−lattice relaxation rate of this single broad line is shown in Figure 11 for the sample with $y = 6$. It shows two distinct transitions around the following temperatures: −10 and 45 °C, which are related to the glass transition and to the strong maximization of the ^{23}Na spin−lattice relaxation rate, respectively. This behavior was observed for all Na^+-doped samples. The effects of the sodium concentration on T_g^{NMR}, T_{max}, and Na^+ ionic conductivity are similar to those observed for Li^+-doped samples.

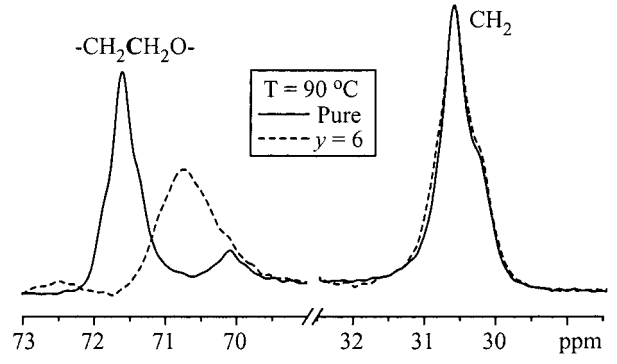

Figure 12. ^{13}C NMR spectra for pure and Li^+-doped ($y = 6$) PEGD, recorded in the viscous liquid phase at 90 °C.

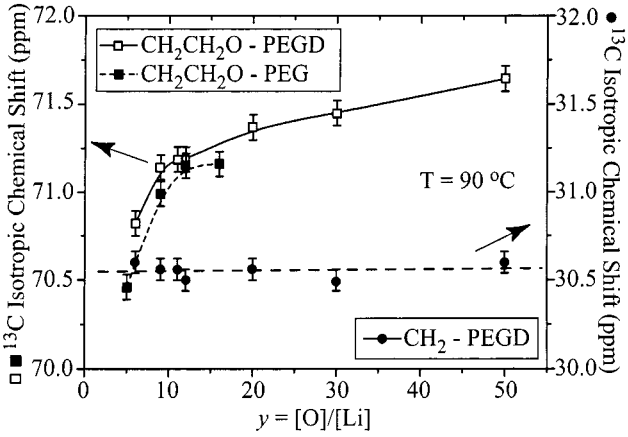

Figure 13. y dependence of the ^{13}C isotropic chemical shift.

^{13}C NMR. Although ^{7}Li and ^{23}Na NMR are important for characterizing the polymer−cation complex dynamics pertaining to ionic conductivity, ^{13}C NMR is better suited for characterizing the polymer−cation interactions and polymer host dynamics. The static direct-polarization ^{13}C NMR spectra for pure and highly Li^+-doped ($y = 5$) PEGD, recorded in the viscous liquid phase at 90 °C, are shown in Figure 12. In both spectra, two main resonances near 30.5 and 71.0 ppm, relative to TMS, are clearly seen. These lines correspond to CH_2 aliphatic carbons, associated with the nonpolar hydrocarbon chains, and to the polar −CH_2**C**H_2O− groups on the ethylene glycol segments, respectively. Weaker resonances related to the less numerous carbon nuclei on the chain ends and connecting sites are also observed but will not be discussed.

A slight decrease of the isotropic chemical shift of the −CH_2**C**H_2O− resonance is the main difference observed due to the presence of the cation Li^+. This effect is consistent with observations in similar polymer ion complexes,[28] where the cation Li^+ is associated with the ether oxygens in the ethylene glycol chain. To further investigate the effects of the lithium concentration on the ^{13}C isotropic chemical shift, this parameter was studied as a function of the oxygen-to-Li^+ ratio, y. The results of these measurements are plotted in Figure 13. For reference, the same measurements were carried out

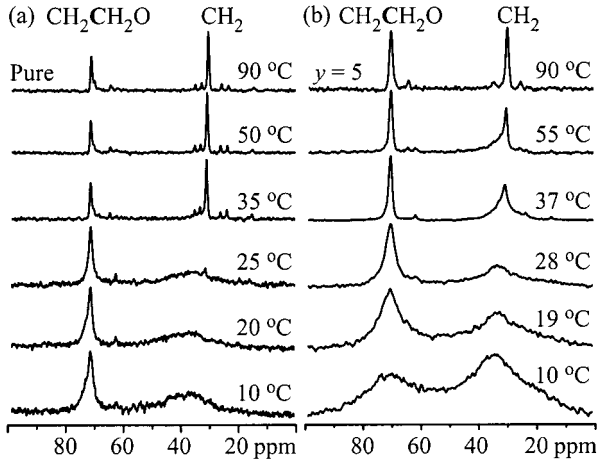

Figure 14. Changes in the line widths of the two ^{13}C resonances $-CH_2\mathbf{C}H_2O-$ and CH_2 as a function of temperature for pure and Li^+-doped ($y = 5$) samples.

for the $-CH_2\mathbf{C}H_2O-$ group of PEG. A small reduction in the $-CH_2\mathbf{C}H_2O-$ carbon isotropic chemical shift of PEGD and PEG is seen to follow the increase in lithium concentration. No modifications are observed for the chemical shift of the CH_2 group of PEGD vs y.

Since the presence of the alkali ion is expected to affect the polymer chain motion, as was observed by the ^7Li line width measurements as a function of the temperature vs y (see Figures 7 and 8), a comparative study was made between the thermal behavior of the pure and the doped PEGD ($y = 5$) samples observing both lines from CH_2 (stearate) and $-CH_2\mathbf{C}H_2O-$ (PEG) groups. Typical spectra at selected temperatures from 10 to 90 °C are shown in Figure 14 for both samples. The higher mobility of the polar ethylene glycol segments is apparent from the behavior of the pure sample near the melting temperature (Figure 14a). In fact, although a single peak in the DSC curve around 35 °C is associated with the melting point of the bulk material, it is clear from the $-CH_2\mathbf{C}H_2O-$ carbon line width that the ethylene glycol segments become highly mobile before the more rigid hydrocarbon structure. A further narrowing of the $-CH_2\mathbf{C}H_2O-$ line, due to the cooperative motion, occurs above the melting of the stearate phase. Figure 14b shows a similar behavior, although in this case the high lithium ion concentration reduces the polar segment motion, making the widths of the two lines comparable below the melting point. At higher temperatures, larger line widths in the $y = 5$ material, relative to pure PEGD, indicate reduced mobility. This is due to the decreased mobility of the PEG segments due to its interaction with Li^+. Below 75 °C, the residual order of the Li^+-doped copolymer, which was observed by the various techniques used in this study, also interferes with complete isotropic averaging of the ^{13}C lines.

Additional significant information obtained from the ^{13}C measurements was the observation of the conformational γ-gauche effect for the methylene groups in the aliphatic PEGD structures.[29] Figure 15 shows the thermal behavior of the isotropic chemical shifts and spin−lattice relaxation rates of both the CH_2 and $-CH_2\mathbf{C}H_2O-$ lines of the sample PEGD with $y = 7$. As can be noted, the melting of the stearate phase occurring around 26 °C is observed not only from the change of the isotropic chemical shift (Figure 15a) but also from

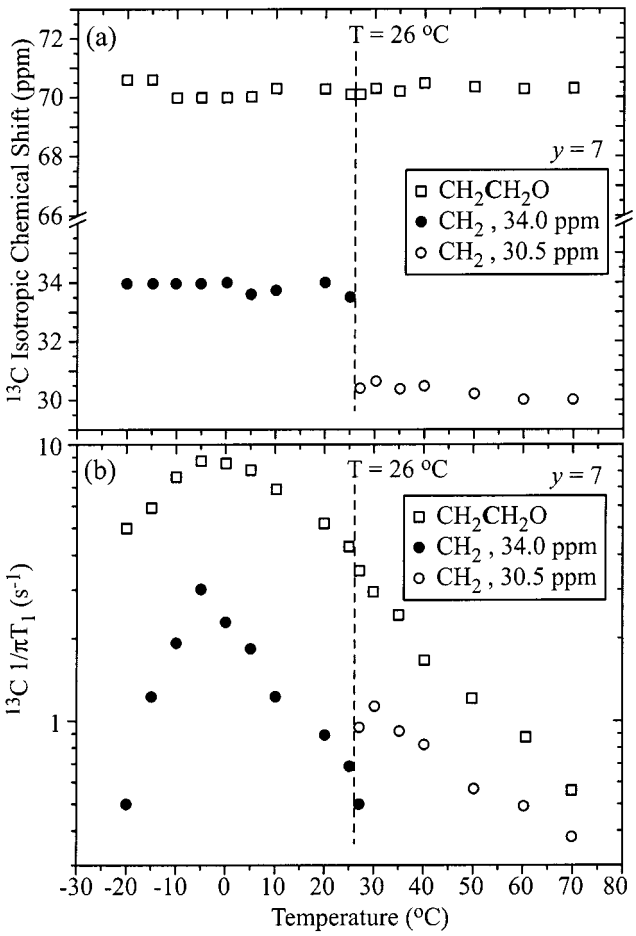

Figure 15. Conformational γ-gauche effect in Li^+-doped PEGD ($y = 7$) observed from ^{13}C isotropic chemical shift and spin−lattice relaxation rate. The $-CH_2\mathbf{C}H_2O-$ ^{13}C isotropic chemical shift and spin−lattice relaxation rate were labeled with different symbols above (○) and below (●) 26 °C in order to distinguish the behavior of both lines.

the strong modification of the spin−lattice relaxation rate (Figure 15b).

^{1}H NMR. ^1H NMR is also useful for characterizing the polymer host dynamics. The static direct-polarization ^1H NMR spectra for the Li^+-doped ($y = 5$) PEGD sample, shown in Figure 16, were recorded for several temperatures above the melting point, from 37 to 90 °C. There are two main lines in the spectrum obtained at 90 °C, near 1.7 and 4.2 ppm relative to TMS. These lines correspond to the CH_2 aliphatic carbons and to the polar $-CH_2\mathbf{C}H_2O-$ groups, respectively. The ^1H spectra observed below the melting point consist of a single broad line and are not shown. As can be seen from the sequence of temperature-dependent spectra in Figure 16, both lines are broad in the temperature interval from 37.0 to 67.5 °C, where ^7Li NMR, SAXS, and DSC data indicate the presence of order in the material. At and above 75 °C, where the material is disordered, both lines become narrower. This indicates that the long-range order below 75 °C inhibits the segmental mobility of the polymer, as also confirmed by ^7Li and ^{13}C NMR. The strong correlation among the ^1H, ^7Li, and ^{13}C NMR temperature-dependent measurements is not unexpected because cation dynamics is promoted by the segmental motion of the polymer host.[12,15−23]

Relation between Microscopic Structure and Ionic Conductivity. With increasing Li^+ concentration, i.e., decreasing y, the ionic conductivity at 50 °C

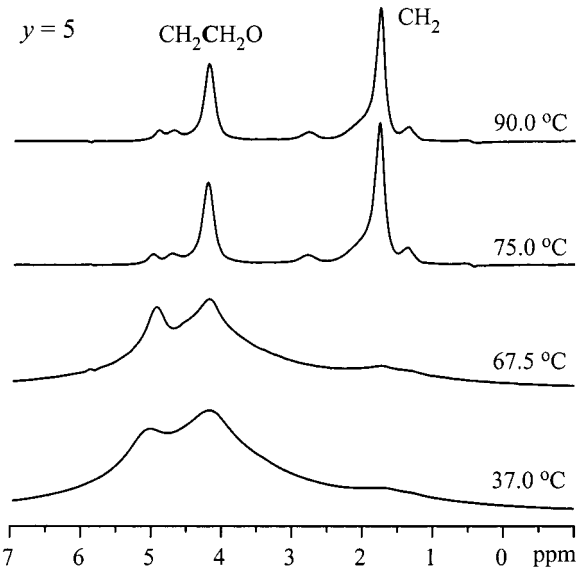

Figure 16. ^{1}H NMR spectra (without sample rotation) for Li^+-doped ($y = 5$) PEGD recorded at 37.0, 67.5, 75.0, and 90 °C.

increases steeply but continuously up to $y = 9$. After that point, it drops abruptly by 40% and decreases further with decreasing y.[4] In this work, we found that at 50 °C an ordered phase is present below $y = 9$. This is evidence that the order in the triblock copolymer decreases the ion diffusivity. This may be due to the tortuosity of the ordered structure and/or due to the reduced segmental mobility in the ordered phase, which was detected by ^{1}H NMR.

Conclusions

Unlike other solid polymer electrolytes,[16] the spectra for highly Li^+-doped PEGD ($y \leq 9$) show sharp ^{7}Li quadrupolar powder patterns even at temperatures well above the polymer melting point. The continued presence of quadrupolar powder patterns is attributed to anisotropic dynamics resulting from order in the triblock copolymer that remains until approximately 72 °C for the sample with $y = 5$, indicating residual dynamic anisotropy in the PEG phase. The residual quadrupole powder pattern is not present in systems over the critical value of $y = 9$. Optical microscopy with polarized light and DSC confirm the presence of order above the melting point for the sample with the highest lithium concentration ($y = 5$). SAXS shows a microphase separation between the melting point and the order−disorder transition at 52 °C for $y = 7$ and 84 °C for $y = 5$. Important for polymer electrolyte applications, the order present in the triblock copolymer with $y < 9$ decreases the segmental mobility, increases the tortuosity, and reduces the ionic conductivity. These results support the use of an order−disorder model[4,5] to explain the previously reported dependence of ionic conductivity on Li^+ concentration in these samples.[1]

Acknowledgment. A. J. Waddon helped with X-ray, J. Morin with DSC, M. Pollard with SAXS, and G. Mantovani with PLM. The authors thank PSE/UMass and DEMA/UFSCar for access to chemistry and/or characterization laboratories and M. R. Pinto, H. Panepucci, and J. P. Donoso for interesting suggestions and/or discussions. The Brazilian agencies FAPESP, CNPq, and FINEP supported this research. Partial support was also provided by NSF/MRSEC at UMass.

References and Notes

(1) deOliveira, A. L.; Damasceno, O. D.; Silva, P. R.; Sangiorge, C. L.; Armand, M.; Kleitz, M. *Solid State Ionics* **1993**, *60*, 99−103.
(2) Bonagamba, T. J.; Giotto, M. V.; Panepucci, H.; deOliveira, A. L.; Sangiorge, C. L. *Bull. Magn. Reson.* **1996**, *17*, 94−95.
(3) Sangiorge, C. L.; Silva, G. G.; deOliveira, A. L.; Pimenta, M.; Damasceno, O. D.; Silva, R. A. *Solid State Ionics* **1996**, *92*, 151−154.
(4) deOliveira, A. L.; Damasceno, O. D.; Silva, P. R.; Sangiorge, C. L.; Donoso, J. P.; Bonagamba, T. J. *Electrochim. Acta* **1997**, *42*, 929−935.
(5) deOliveira, A. L.; Silva, P. R. *Electrochim. Acta* **1998**, *43*, 693−699.
(6) Roux, C.; Gorecki, W.; Sanchez, J. Y.; Jeannin, M.; Belorizky, E. *J. Phys.: Condens. Matter* **1996**, *8*, 7005−7017.
(7) Slichter, C. P. *Principles of Magnetic Resonance*, 3rd ed.; Springer-Verlag: Heidelberg, Germany, 1990; Vol. 1.
(8) Bloembergen, N.; Purcell, E. M.; Pound, R. V. *Phys. Rev.* **1948**, *73*, 679−712.
(9) Gutowski, H. S.; Pake, G. E. *J. Chem. Phys.* **1950**, *18*, 162−170.
(10) Boyce, J. B.; Huberman, B. A. *Phys. Rep.* (Review Section of *Phys. Lett.*) **1979**, *51*, 189−265.
(11) Hendrickson, J. R.; Bray, P. J. *J. Magn. Reson.* **1973**, *9*, 341−357.
(12) Chung, S. H.; Jeffrey, K. R.; Stevens, J. R. *J. Chem. Phys.* **1991**, *94*, 1803−1811.
(13) Berger, S.; J., R.; Brinkmann, D.; Chowdari, B. *Solid State Ionics* **1996**, *86−88*, 475−479.
(14) Cocciantelli, J.; Suh, K.; Sénégas, J.; Doumerc, J.; Pouchard, M. *J. Phys. Chem. Solids* **1992**, *53*, 857−859.
(15) Berthier, C.; Gorecki, W.; Minier, M.; Armand, M. B.; Chabagno, J. M.; Rigaud, P. *Solid State Ionics* **1983**, *11*, 91−95.
(16) Donoso, J. P.; Bonagamba, T. J.; Panepucci, H. C.; Oliveira, L. N.; Gorecki, W.; Berthier, C.; Armand, M. *J. Chem. Phys.* **1993**, *98*, 10026−10036.
(17) Brown, S. D.; Greenbaum, S. G.; McLin, M. G.; Wintersgill, M. C.; Fontanella, J. J. *Solid State Ionics* **1994**, *67*, 257−262.
(18) Schantz, S.; Maunu, S. L. *Macromolecules* **1994**, *27*, 6915−6921.
(19) Johansson, A.; Gogoll, A.; Tegenfeldt, J. *Polymer* **1996**, *8*, 1387−1393.
(20) Johansson, A.; Tegenfeldt, J. *J. Chem. Phys.* **1996**, *104*, 5317−5325.
(21) Wong, S.; Vaia, R. A.; Gianellis, E. P.; Zax, D. B. *Solid State Ionics* **1996**, *86−88*, 547−557.
(22) Mello, N. C.; Bonagamba, T. J.; Panepucci, H.; Dahmouche, K.; Judeinstein, P.; Aegerter, M. A. *Macromolecules* **2000**, *33*, 1280−1288.
(23) de Souza, P. H.; Bianchi, R. F.; Dahmouche, K.; Judeinstein, P.; Faria, R. M.; Bonagamba, T. J. *Chem. Mater.* **2001**, *13*, 3685−3692.
(24) Druger, S. D.; Nitzan, A.; Ratner, M. A. *J. Chem. Phys.* **1983**, *79*, 3133−3142.
(25) Bianchi, R. F.; Souza, P. H.; Bonagamba, T. J.; Panepucci, H. C.; Faria, R. M. *Synth. Met.* **1999**, *102*, 1186−1189.
(26) Pietrass, T.; Burkert, P. K. *Magn. Reson. Chem.* **1993**, *31*, 709−713.
(27) Halstead, T. K. *J. Chem. Phys.* **1970**, *53*, 3427−3435.
(28) Müller-Plathe, F.; van-Gunsteren, W. F. *J. Chem. Phys.* **1995**, *103*, 4745−4756.
(29) Tonelli, A. E. *NMR Spectroscopy and Polymer Microstrucure: The Conformational Connection*; VCH Publishers: New York, 1989.

MA010515Q